Redox Biology 46 (2021) 102111

Contents lists available at ScienceDirect

Redox Biology

journal homepage: www.elsevier.com/locate/redox

Mass spectrometry-based direct detection of multiple types of protein thiol modifications in pancreatic beta cells under endoplasmic reticulum stress

Xiaolu Li [a,1], Nicholas J. Day [b,1], Song Feng [b], Matthew J. Gaffrey [b], Tai-Du Lin [b], Vanessa L. Paurus [b], Matthew E. Monroe [b], Ronald J. Moore [b], Bin Yang [a], Ming Xian [c], Wei-Jun Qian [b,*]

[a] Department of Biological Systems Engineering, Washington State University, Richland, WA, 99354, USA
[b] Biological Sciences Division, Pacific Northwest National Laboratory, Richland, WA, 99352, USA
[c] Department of Chemistry, Brown University, Providence, RI, 02912, USA

ARTICLE INFO

Keywords:
Protein thiols
Thiol redox modifications
Direct detection
Post-translational modifications
Redox proteomics

ABSTRACT

Thiol-based post-translational modifications (PTMs) play a key role in redox-dependent regulation and signaling. Functional cysteine (Cys) sites serve as redox switches, regulated through multiple types of PTMs. Herein, we aim to characterize the complexity of thiol PTMs at the proteome level through the establishment of a direct detection workflow. The LC-MS/MS based workflow allows for simultaneous quantification of protein abundances and multiple types of thiol PTMs. To demonstrate its utility, the workflow was applied to mouse pancreatic β-cells (β-TC-6) treated with thapsigargin to induce endoplasmic reticulum (ER) stress. This resulted in the quantification of >9000 proteins and multiple types of thiol PTMs, including intra-peptide disulfide (S–S), S-glutathionylation (SSG), S-sulfinylation (SO_2H), S-sulfonylation (SO_3H), S-persulfidation (SSH), and S-trisulfidation (SSSH). Proteins with significant changes in abundance were observed to be involved in canonical pathways such as autophagy, unfolded protein response, protein ubiquitination pathway, and EIF2 signaling. Moreover, ~500 Cys sites were observed with one or multiple types of PTMs with SSH and S–S as the predominant types of modifications. In many cases, significant changes in the levels of different PTMs were observed on various enzymes and their active sites, while their protein abundance exhibited little change. These results provide evidence of independent translational and post-translational regulation of enzyme activity. The observed complexity of thiol modifications on the same Cys residues illustrates the challenge in the characterization and interpretation of protein thiol modifications and their functional regulation.

1. Introduction

Post-translational modifications (PTMs) on protein cysteine thiols have been widely reported for their significance in redox signaling and regulation mediated by reactive oxygen/nitrogen/sulfur species (ROS/RNS/RSS) [1]. The formation of these redox-dependent PTMs on protein thiols through different chemistry and reactants, results in multiple types of reversible modifications including disulfide, S-glutathionylation (SSG), S-sulfenylation (SOH), S-nitrosylation (SNO), S-persulfidation (aka. S-sulfhydration), and S-polysulfidation ($S\text{-}(S)_n\text{-}H$, $n \geq 1$) [2–4]. These reversible modifications may be reduced to free thiols by antioxidant systems, thus impacting enzymatic activities and conformation of individual proteins to modulate downstream biological processes (e.g. cell metabolism, survival/death, inflammation, endoplasmic reticulum stress) in response to redox signals [5,6]. On the contrary, irreversible modifications such as S-sulfinylation (SO_2H) and S-sulfonylation (SO_3H) are formed by disulfide oxidation [7] or continued oxidation of SOH, and these modifications are often considered as markers of oxidative stress-related pathogenesis [8]. It should be noted that a subset of SO_2H modification on proteins such as 2-Cys peroxiredoxins can be selectively reduced back to free thiols by sulfiredoxin (Srx), supporting the regulatory role of this modification on protein function [9]. The ability to accurately measure the extent and types of thiol PTMs that occur following a perturbation are critical for a better understanding of the role of thiol PTMs in altering cellular responses through regulating protein function and activity.

Previous work has illustrated that the oxidation profiles can be

* Corresponding author. PO Box 999, MSIN K8-98, Biological Science Division, Pacific Northwest National Laboratory, Richland, WA, 99352, USA.
E-mail address: weijun.qian@pnnl.gov (W.-J. Qian).
[1] These authors contributed equally to this work.

https://doi.org/10.1016/j.redox.2021.102111
Received 2 July 2021; Received in revised form 16 August 2021; Accepted 16 August 2021
Available online 17 August 2021

Abbreviations

AARS1	Alanine–tRNA ligase, cytoplasmic
ATF4	Cyclic AMP-dependent transcription factor ATF-4
ATF6	Cyclic AMP-dependent transcription factor ATF-6 alpha
ATG13	Autophagy-related protein 13
ATG14	Beclin 1-associated autophagy-related key regulator
ATR	Serine/threonine-protein kinase ATR
BST	Biotin-switch technique
CARS1	Cysteine–tRNA ligase, cytoplasmic
CEBPB	CCAAT/enhancer-binding protein beta
CEBPG	CCAAT/enhancer-binding protein gamma
CISD1	CDGSH iron-sulfur domain-containing protein 1
COF1	Cofilin-1
DDIT3	DNA damage-inducible transcript 3 protein
DNAJA3	DnaJ homolog subfamily A member 3, mitochondrial
DNAJA4	DnaJ homolog subfamily A member 4
DTT	Dithiothreitol
EIF1A	Eukaryotic translation initiation factor 1A
EIF2B2	Translation initiation factor eIF-2B subunit beta
EIF2S2	Eukaryotic translation initiation factor 2 subunit 2
EIF3J	Eukaryotic translation initiation factor 3 subunit J-A
EIF5	Eukaryotic translation initiation factor 5
EIF5B	Eukaryotic translation initiation factor 5B
EPG5	Ectopic P granules protein 5 homolog
EPRS1	Bifunctional glutamate/proline–tRNA ligase
ER	Endoplasmic reticulum
ERAD	ER-associated protein degradation
ERN1	Serine/threonine-protein kinase/endoribonuclease IRE1
ERO1A	ERO1-like protein alpha
FDR	False discovery rate
GAPDH	Glyceraldehyde 3-phosphate dehydrogenase
GARS1	Glycine–tRNA ligase
GDH1	Glutamate dehydrogenase 1
HPE-IAM	β-(4-hydroxyphenyl)ethyl iodoacetamide
HSPA5	Endoplasmic reticulum chaperone BiP
HSPA9	Stress-70 protein, mitochondrial
LARS1	Leucine–tRNA ligase, cytoplasmic
NARS1	Asparagine–tRNA ligase, cytoplasmic
NEM	N-Ethylmaleimide
P4HB	Protein disulfide-isomerase
PTM	Post-translational modifications
RAC	Resin-assisted capture
ROS/RNS/RSS	Reactive oxygen/nitrogen/sulfur species
SNO	S-nitrosylation
SO_2H	S-sulfinylation
SO_3H	S-sulfonylation
SOH	S-sulfenylation
SQSTM	Sequestosome-1
S–S	Intra-peptide disulfide
SSG	S-glutathionylation
SSH	S-persulfidation
SSSH	S-trisulfidation
Tg	Thapsigargin
UCHL1	Ubiquitin C-terminal hydrolase L1
UPR	Unfolded protein response
VARS1	Valine–tRNA ligase
VARS2	Valine–tRNA ligase, mitochondrial
WARS1	Tryptophan–tRNA ligase, cytoplasmic
YARS1	Tyrosine–tRNA ligase, cytoplasmic

comprised of multiple types of PTMs on individual amino acid residues, including Cys, Tyr, and Trp [10–12]. For example, Tyr can be oxidized to 3,4-dihydroxyphenylalanine (DOPA), dopaquinone (DQ), and diTyr mediated by $^{\bullet}$OH or other redox-active species [10,13]. However, there is relatively limited knowledge of multiple modifications occurring at a single site of a given protein under physiological conditions. The catalytic site of glyceraldehyde 3-phosphate dehydrogenase (GAPDH) is one such example, where research has found that GAPDH is subjected to multiple types of oxidative modifications, each having a different effect on protein function [14,15]. Studies on plant or rabbit muscle GAPDH indicate that SNO and SOH of the catalytic Cys site have inhibitory effects on GAPDH function [16,17]. These modifications can be transformed to SSG, which is a reversible modification recognized for its protective role in preventing over-oxidation of protein thiols into irreversible modifications [17,18]. Furthermore, a recent report identified a switch from SSG to SSH on the same cysteine site under oxidative stress, which was suggested as a potential mechanism to tune cellular energy metabolism [19]. These findings support the notion that redox regulation of protein function and subsequent signaling and biological processes is a complex, yet 'finely tuned' process through the diversiform of thiol PTMs and their dynamics under perturbations.

The complexity and interplay of multiple forms of thiol PTMs at the same Cys site is an important aspect of protein regulation, as these changes modulate protein function and influence downstream biological processes. Despite a relatively good understanding of the individual types of thiol PTMs, identification of more than one PTM at the same Cys site and knowledge of how different PTM distributions dictate protein function is limited. Profiling for multiple types of redox PTMs at the site-specific level would enable a broad view of the landscape of thiol PTMs and potential crosstalk between redox signaling pathways and their regulation via redox switches. In this study, we aim to further explore how perturbations of the redox state can be seen through Cys sites that exhibit a dynamic distribution of various forms of thiol PTMs.

Recently, mass spectrometry (MS)-based proteomics approaches have rapidly advanced to enable proteome-wide site-specific characterization of various redox PTMs. Due to the labile nature and low abundance of redox PTMs, the majority of current approaches are indirect and rely on selective reduction of a single type of redox PTM or total thiol oxidation (i.e., all reversible forms of thiol PTMs) as a whole to enrich the specific types of modifications of interest [20–27]. The most common methods of indirect detection are the biotin-switch technique (BST) [28] and resin-assisted capture (RAC) [21,29]. In general, all free thiols are first blocked by an alkylating agent, followed by reduction of targeted redox PTMs with specific reductants (e.g. glutaredoxin 1 for reducing SSG, ascorbate combined with Cu^{+}/Cu^{2+} for reducing SNO). Then, the nascent free thiols can be tagged with thiol-specific biotinylating reagents to be enriched by avidin, or directly enriched by thiol-affinity resin, which are further subjected to MS analysis. These assays provide relatively robust profiling of specific types of redox PTMs, enabling identification of individual types of modifications relevant to various physiological states and processes. However, the major caveat of these indirect approaches is that typically only one type of redox PTM may be profiled in a given study, leaving an incomplete view of the diverse landscape of redox PTMs.

To explore the complex and multiform redox PTM landscape in a biological system, we devised a MS-based direct detection workflow without enrichment steps to enable simultaneous quantitative profiling of the global proteome and multiple types of thiol PTMs in a single experiment. Using pancreatic β-cells under ER stress as a model system for a perturbed cellular redox state, we hypothesize that cysteine site PTM profiles are diversified by multiple forms of thiol PTMs that induce specific biological responses to oxidative stress. The conceptual advantage of the direct detection strategy was recently demonstrated in the profiling of persulfidation [30]. Given the reported potential instability

of protein persulfidation and polysulfidation (S-(S)$_n$-H, n ≥ 1) [31], we evaluated an alternative alkylation agent, β-(4-hydroxyphenyl)ethyl iodoacetamide (HPE-IAM), for blocking reactive thiol groups including hydropolysulfides based on its reported mild electrophilicity to generate comparably stable adducts with hydropolysulfides [32]. Using this deep proteome profiling strategy, we are able to investigate the distribution of multiple types of thiol PTMs (intra-peptide disulfide (S–S), SSG, SO_2H, SO_3H, SSH, and SSSH) in pancreatic β-cells undergoing endoplasmic reticulum (ER) stress. This work demonstrated the presence of a variety of thiol modifications with many of them on the same cysteine residues and exhibiting different combinatorial modifications on closely located cysteine sites. Our study emphasizes the complexity of redox PTMs and their regulation in biological systems, as revealed by evidence of proteins displaying distinctive changes in protein abundances and PTM levels.

2. Materials and methods

2.1. Cell line and cell culture

Mouse pancreatic β-cells (β-TC-6) (ATCC# CRL-11506) were cultured in RPMI-1640 containing 15% FBS, 11.1 mM glucose, 1 mM glutamine, and 1% anti-biotic/mycotic [22]. RAW 264.7 (ATCC # TIB-71) cells were cultured in RPMI-1640 supplemented with 10% FBS, 2 mM L-glutamine (Fisher Scientific, Rockford, IL), and 1% penicillin–streptomycin (Fisher Scientific, Rockford, IL) [33]. The cells were maintained in a humid incubator at 37 °C with 5% CO_2. Prior to treatment, both β-TC-6 cells and RAW 264.7 cells were seeded into 100 mm culture plates and grown until 60% confluent. To induce ER stress, original growth media was removed and replaced with media containing 400 nM thapsigargin (Tg) for an additional 18 h [22,34]. Cell culture without Tg treatment was used as a control experiment. Five biological replicates were used for both control and Tg-treated experiment.

2.2. Resin-assisted capture (RAC) of protein thiols to evaluate alkylation reagents

To evaluate the alkylation efficiency of HPE-IAM versus NEM, the RAC protocol was applied to capture proteins containing non-alkylated thiols. RAW 264.7 mouse macrophage cells were rinsed twice with PBS buffer (pH 7.4) and harvested in lysis buffer A (250 mM HEPES, 10 mM EDTA, 1% Triton X-100, pH 7.5) containing HPE-IAM (1, 5, 10, or 15 mM) or lysis buffer B (250 mM MES, 10 mMEDTA, 1% Triton X-100, pH 6.0) containing NEM (10 or 100 mM). Lysis buffer B containing no alkylation agent was used as a control experiment. Cell lysates were centrifuged at 16,000 g for 10 min at 4 °C to remove cell debris. HPE-IAM-alkylation was carried out at 37 °C while NEM alkylation was carried out at 55 °C. Both reactions were conducted in the dark with 2% SDS for 30 min, followed by acetone precipitation overnight at −20 °C. Protein pellets were washed with acetone twice then re-suspended in 250 mM HEPES containing 8 M urea and 0.1% SDS (pH 7.0). All protein samples were reduced with 20 mM dithiothreitol (DTT), followed by buffer exchange to 25 mM HEPES (pH 7.0) containing 1 M urea and 0.1% SDS. Protein concentration was measured by bicinchoninic acid (BCA) assay. 150 μg protein from each sample was transferred to preconditioned thiol-affinity resin (Thiopropyl Sepharose 6B resin, 30 mg/column) for 2h enrichment in 120 μL of 25 mM HEPES buffer (pH 7.7) containing 0.1% SDS. The detailed experimental condition for resin-assisted enrichment of proteins containing free thiols is described elsewhere [35,36]. Briefly, after enrichment, unbound proteins containing no free thiols were washed off. Proteins covalently bound on resin were digested with trypsin, followed by another wash to remove non-cysteine peptides. 20 mM DTT was used to elute cysteine-containing peptides. The enriched peptide samples were stored at −20 °C before SDS-polyacrylamide gel electrophoresis.

2.3. SDS-polyacrylamide gel electrophoresis (SDS-PAGE)

SDS-PAGE was carried out using a 4%–12% (w/v) precast linear gradient Tris-HCl polyacrylamide gel (Bio-Rad) to compare the enriched peptide amount using different types and concentrations of alkylation reagents. Equal volumes (15.6 μL) of the above cysteine-containing peptide samples and LDS loading buffer were mixed and incubated at 70 °C for 10 min with 50 mM DTT. 6 μL of See Blue Plus 2 protein standard was loaded onto the gel. Gel electrophoresis was run at 120 V for 30 min in Tris/glycine/SDS buffer (Bio-Rad), followed by silver staining according to the manufacturer's instructions (Thermo Scientific).

2.4. Sample preparation for LC-MS/MS evaluation of alkylation reagents

RAW 264.7 cells were rinsed twice with PBS buffer without calcium and magnesium and harvested in lysis buffer A (250 mM HEPES, 10 mM EDTA, 0.1 mM neocuproine, 1% Triton X-100, 8 M urea, pH 7.5) containing 10 mM HPE-IAM, or lysis buffer B (250 mM MES, 10 mM EDTA, 0.1 mM neocuproine, 1% Triton X-100, pH 6.0) containing 10 mM NEM. Cell lysates were spun down at 16,000 g, at 4 °C for 10 min to collect protein in supernatant. HPE-IAM and NEM alkylation was conducted with 2% SDS at 37 °C and 55 °C, respectively, in the dark for 30 min, followed by acetone precipitation. For HPE-IAM alkylated samples, the protein pellet was resuspended in 250 mM HEPES (pH 7.5) containing 8 M urea and 5 mM HPE-IAM, then incubated at 37 °C in the dark for 30 min to ensure all free thiols were alkylated. Protein pellets of NEM-alkylated samples were resuspended in 250 mM HEPES (pH 7.5) containing 8 M urea. Protein concentration was measured by BCA. 100 μg protein from each sample was subjected to trypsin digestion at 37 °C for 3 h. The samples were desalted with C18 SPE Clean-up column (Agilent technologies, Santa Clara, CA) and concentrated by a SC110 Speed Vac (ThermoSavant, Holbrook, NY). Samples were reconstituted with 30 μL 0.1% formic acid. The final protein concentration of each sample was 0.1 μg/μL for LC-MS/MS analysis. Three biological replicates were used for each alkylation condition.

2.5. Sample preparation for direct detection of protein thiol modifications

After treatment, β-TC-6 cells were rinsed twice with PBS buffer without calcium and magnesium and harvested in lysis buffer (250 mM HEPES, 10 mM EDTA, 0.1 mM neocuproine, 1% Triton X-100, 8 M urea, pH 7.5) containing 10 mM HPE-IAM. Cell lysates were centrifuged at 16,000 g, at 4 °C for 10 min to collect protein in supernatant. Subsequently, alkylation was conducted with 2% SDS at 37 °C in the dark for 30 min, followed by acetone precipitation. The protein pellet was resuspended in 250 mM HEPES (pH 7.5) containing 5 mM HPE-IAM and 8 M urea and incubated at 37 °C in the dark for 30 min. Protein concentration was measured by BCA. 100 μg protein from each sample was subjected to trypsin digestion at 37 °C for 3 h. The samples were cleaned up with C18 SPE Clean-up column and concentrated by a SC110 Speed Vac. Peptides were then labeled with TMT10-plex (Pierce Biotechnology, Rockford, IL) following the manufacturer's instructions. The samples were pooled together, cleaned up, and concentrated again. The purified peptides were dissolved in a solution containing 3% acetonitrile; 97% ultrapure water and quantified by BCA. 40 μg of peptide was fractionated using a reversed-phase Phenomenex Jupiter C18 column (65 cm × 200 μM internal diameter (ID) packed with 3 μm particles) on a nanoAcquity ultra performance liquid chromatography (UPLC) system (Waters). Binary solvent buffers (~pH 7) are comprised of mobile phase A (10 mM ammonium formate in water) and mobile phase B (acetonitrile). Peptides were separated using a gradient applied as follows: 35 min with buffer A, and then separated with buffer B from 1% to 10% in 2 min, 15 min to 15%, 35 min to 25%, 25 min to 35%, 13 min to 45%, and 43 min to 90%. The column was washed with 90% B for min and returned back to 99% A in 10 min. Eluted peptides were separated into

96 fractions in 1-min intervals, which were concatenated into 24 fractions using a HTC PAL autosampler (CTC analytics) running Chronos software. The flow rate was kept at 2.2 μL/min. Fractions were dispensed into wells of a 96 well plate containing 20 μL of 0.03% N-Dodecyl-β-maltoside to facilitate collection and prevent peptide loss. Samples were stored frozen until second-dimension low pH LC-MS/MS.

2.6. LC-MS/MS analysis

LC–MS/MS analysis was performed was performed as previously described [37]. Briefly, LC-MS/MS was performed using a nanoAcquity UPLC system (Waters) coupled to a Q-Exactive HF-X Orbitrap Mass Spectrometer (Thermo Scientific, San Jose, CA) with a 120-min LC gradient. Full MS spectra were recorded at resolution of 60 K with an automated gain control (AGC) value of 3e6. Data were acquired with a full MS scan over the range of *m/z* 300–1800. MS/MS was performed in a data dependent mode (DDA) at a resolution of 45 K. The most abundant 12 parent ions were selected for MS/MS using high-energy collision dissociation (HCD) with a normalized collision energy setting of 30. Precursor ion activation was performed with an isolation width of 0.7 Da. The AGC target value for MS/MS scans was 1e5. Dynamic exclusion time was set at 45 s.

2.7. Data analysis

LC-MS/MS raw data converted into dta files using Bioworks Cluster 3.2 (Thermo Fisher Scientific, Cambridge, MA) and the MS-GF + algorithm [38] (v2021.03.22) was used to search MS/MS spectra against the FASTA files of Mus musculus Uniprot database (released in 2017-04-12) using the following parameters: Parent ion tolerance was ± 20 ppm; Static 10-plex TMT modification of lysine and N-termini of peptides (229.1629 Da); Dynamic modification setup included oxidation of methionine (15.9949 Da), HPE-IAM modification on free thiol (177.0790 Da), persulfide with HPE-IAM (SS-HPE-IAM, 209.0510 Da) or trisulfides (SSS-HPE-IAM, 241.0231 Da), S-glutathionylation (SSG, 305.0681 Da), S-sulfinylation (SO_2H, 31.9898 Da), S-sulfonylation (SO_3H, 47.9847 Da), and intra-peptide disulfide (S–S, −1.0078 Da on each Cys residue). Partially tryptic termini were used for searching. The spectral level false discovery rate (FDR) was ≤1% based on a target-decoy searching strategy. Peptide identification was filtered by MSGFDB SpecEvalue < 1E–9, –10 < DelM_ppm <10, PepQvalue <0.01 to control FDR at global level ~1%. TMT reporter ion intensities of peptides were normalized, summed, and log2 transformed for corresponding protein abundance quantification.

For PTM level data, reporter ion intensities of peptides with same sequences and modifications were summed to quantify unique peptides with modifications. To control the FDR for PTM-containing peptides, all unique cysteine-containing peptides were filtered by the following criteria: at least two forms were found on the same Cys sites including alkylated SH (unmodified form), SSH, SSSH, SSG, SO_2H, SO_3H, or S–S. This filtering step was combined with filtering by MSGFDB SpecEvalue < 1E–10 to control the FDR at PTM level to be <1%. The peptides are mapped with protein sequences to get the Cys site locations. Each of the peptide-containing Cys are annotated with site location on the protein and its modification form. After the filtering steps, intensities of peptides with the same modification forms on the same Cys sites or motifs were aggregated to quantify the modifications at site level. Student t-test was applied to compare the levels of protein expression or thiol modifications. The Benjamini-Hochberg adjusted p-value was calculated to control the false discovery rate (FDR) among comparison [39,40]. The statistically significant changes of protein expression and thiol modification between Tg-treated and control samples were identified when adjusted p-value < 0.05 and 0.15, respectively. The heatmaps of the protein levels and PTM levels were generated from median centered intensity values for each protein or each protein PTM form using an R script and ggplot2 package. Ingenuity Pathway Analysis (IPA) (QIAGEN Inc) core analysis [41] was applied to analyze canonical pathways for both the global protein expression data and thiol PTM data. Cysteine sites were highlighted in protein structures using ICM-Browser Pro.

2.8. Data availability

The raw datasets presented in this study can be found in online repositories. The names of the repository/repositories and accession number(s) can be found below: Massive.ucsd.edu with accession: MSV000087543. The data will also be available through ProteomeXchange with accession: PXD026358.

3. Results

3.1. Assessment of the direct detection method for profiling thiol PTMs

Conceptually, all types of protein thiol PTMs are potentially identifiable by shotgun LC-MS/MS, provided that the modifications can be preserved during sample processing and MS analyses and their abundance is sufficient for MS detection. Following this notion, we devised a workflow (Fig. 1A), relying on efficient blocking of all reactive thiols, including both free thiols (-SH) and hydropolysulfides (-S-$(S)_n$-H, $n \geq 1$), which are prone to being oxidized or altered during sample processing. Most types of thiol PTMs including SSG, SO_2H, SO_3H, and disulfides are relatively stable during sample processing or LC-MS/MS analyses, while SOH and SNO are labile (prone to further reactions and degradation) [42,43]. Following blocking of reactive thiols, multiple types of the above-mentioned stable thiol PTMs may be detected directly by LC-MS/MS profiling without enriching specific types of PTMs.

In developing our workflow, we were concerned about the stability of protein hydropolysulfides during the alkylation step. Recently, Bogdándi et al. reported that the use of a strong alkylation agent such as N-Ethylmaleimide (NEM) can cleave polysulfur chains of small-molecular-weight polysulfur species (e.g. glutathione polysulfides, G$(S)_n$G, $n > 2$) and polysulfide species on GAPDH while β-(4-hydroxyphenyl) ethyl iodoacetamide (HPE-IAM) is an alkylation reagent that largely preserves polysulfides [31]. Built upon this observation, we evaluated NEM and HPE-IAM as two alkylation reagents (Fig. 1B), where HPE-IAM was previously highlighted for its mild electrophilicity to generate comparably stable adducts with hydropolysulfides. It was reported that compared to commonly used NEM, HPE-IAM had a potent protective effect on various cellular small-molecular-weight polysulfides against degradation via cleavage of sulfur bonds [44]. However, this alkylation agent has not been well evaluated for proteomics applications, while NEM is commonly used to block free thiols quickly to avoid possible artificial oxidation of free thiols during processing [29]. Thus, we compared different concentrations of HPE-IAM and NEM for their efficiency in blocking free thiols and the preservation of protein polysulfides.

All initial method assessments were performed using mouse RAW 264.7 macrophage cells. During cell lysis, 1, 5, 10, 15 mM HPE-IAM or 10, 100 mM NEM was included for blocking reactive thiols for 30 min (Fig. 1C). Given our interest in identifying protein S-polysulfidation modifications, the selection of the range of concentrations and reaction conditions were based on previous studies for stabilization of polysulfides, with some potential compromise for alkylation efficiency [32,44]. To assess alkylation efficiency, we enriched all proteins that contained either unblocked free thiols (due to incomplete alkylation) or reversibly oxidized thiols by treating protein samples with 20 mM DTT. Following resin-assisted capture (RAC) of thiol-containing proteins and on-resin trypsin digestion, the final cysteine (Cys)-containing peptides were eluted by DTT for SDS-PAGE. 100 mM NEM as an alkylation reagent clearly showed the best alkylation efficiency since it had the least number of Cys-containing peptides (from either formerly oxidized thiols or unblocked free thiols) enriched by RAC (Fig. 1C). On the contrary, 1 mM HPE-IAM had the least visible effect on blocking free thiols while 10

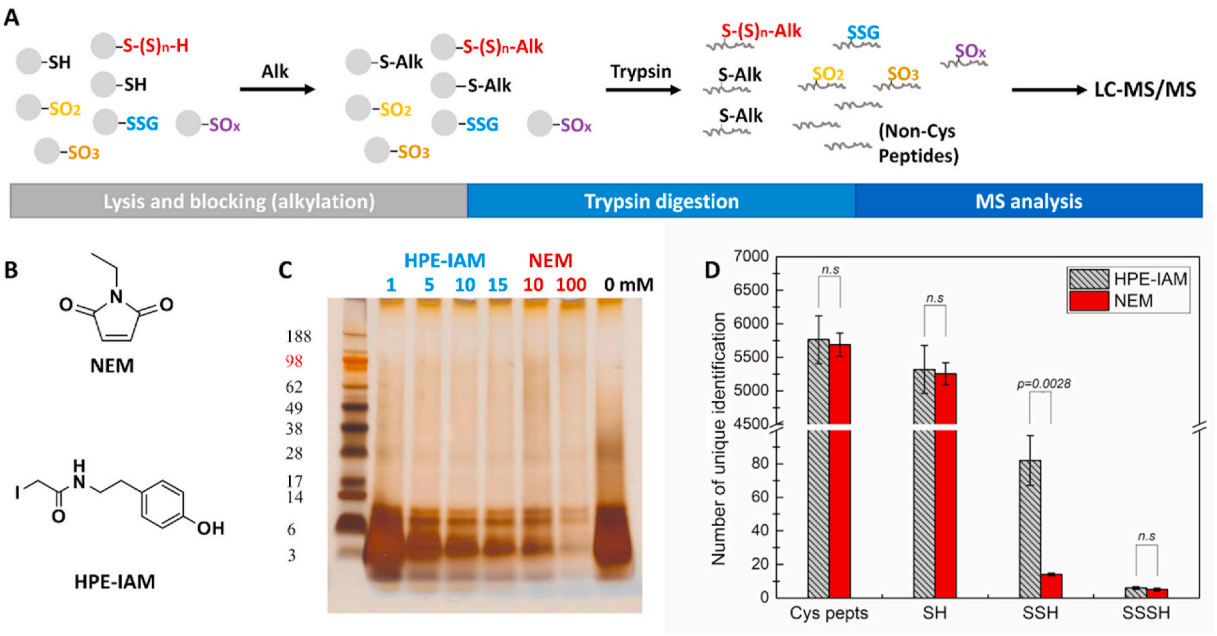

Fig. 1. Assessment of a direct detection workflow for thiol PTM profiling. (A) Workflow schematics: 1) cell lysis and blocking (alkylation); 2) trypsin digestion. Free thiols, –SH; S-polysulfidation, -S-(S)$_n$-H; S-glutathionylation, -SSG; S-sulfinylation, –SO_2; S-sulfonylation, –SO_3; Other forms of thiol modification, -SOx; Alkylation, Alk. (B) Alkylation reagents used in the workflow. (C) Evaluation of alkylation efficiency of HPE-IAM and NEM via RAC protocol. 0 mM (without alkylation agent) was used as a control experiment. (D) Number of unique peptides in RAW cells alkylated by 10 mM HPE-IAM or 10 mM NEM. Cys pepts, total cysteine-containing peptides; SH, peptides containing alkylated cysteine thiols; SSH, peptides containing alkylated persulfides; SSSH, peptides containing alkylated trisulfides.

mM HPE-IAM and 10 mM NEM displayed comparable blocking efficiency in reducing the amounts of Cys-containing peptides that are enriched.

Next, we compared the differences in 10 mM HPE-IAM and 10 mM NEM as two alkylation conditions in preserving endogenous protein S-polysulfidation as assessed by LC-MS/MS. Protein samples after blocking of reactive thiols were directly subjected to trypsin digestion without further reduction and analyzed by LC-MS/MS. The average number of all unique peptides containing cysteines, alkylated unmodified cysteines (-SH), and alkylated polysulfides (-SSH and –SSSH) from three replicates were compared to assess the effect of alkylation on the detectability of polysulfides (Fig. 1D). The numbers of total Cys-containing peptides (~5700) and unmodified Cys-containing (SH) peptides (~5300) were comparable for both HPE-IAM and NEM as alkylation reagents. The alkylation efficiency was similarly high for both reagents with only ~1% Cys-containing peptides identified as unblocked free thiols. However, the number of SSH containing peptides identified were much lower in NEM samples compared to HPE-IAM samples. The results are consistent with the previous observation that NEM is a strong alkylation reagent, which can cleave polysulfur chains [31]. The number of SSSH containing peptides identified were too low to see a clear difference between the two alkylation reagents. Together, these results demonstrated that HPE-IAM not only provided good alkylation efficiency for reactive thiols, but is also much better at preserving persulfides. Thus, 10 mM HPE-IAM was selected as the condition for the initial blocking step to efficiently block reactive thiols and preserve polysulfide modifications in the direct detection workflow.

3.2. *Simultaneous quantitative profiling of the global proteome and multiple types of thiol PTMs*

One of our interests is to reveal the distinctive translational and redox-dependent posttranslational regulatory mechanisms through PTMs in pancreatic beta-cells under ER stress by applying the direct detection method. Since the direct detection method does not involve any enrichment of PTMs, the shotgun profiling will allow simultaneous measurements of both protein and PTM abundances. To facilitate multiplexed quantification with a deep proteome coverage, we have incorporated isobaric TMT labeling (10-plex) and high pH reversed phase LC fractionation (Fig. 2A). This workflow enabled comparison between the control and ER stress conditions of β-cells (n = 5 biological replicates) induced by 400 nM thapsigargin (Tg) [22]. In total, 126,531 unique peptides covering 9342 proteins were quantitatively measured (Fig. 2B, Table S1), reflecting a relatively deep proteome coverage for β-cells. Fig. 2C further summarizes the overall coverage of total unique Cys-containing peptides and peptides containing different types of thiol PTMs, including SSH and SSSH (alkylated by HPE-IAM), SSG, SO_2H, SO_3H, and intra-peptide disulfide (S–S). All modifications were identified with FDR controlled at <1% for each type of modification (see Methods). We also note that while it is technically difficult to identify inter-peptide disulfides using shotgun proteomics, it is possible to identify intra-peptide disulfides (i.e., two Cys residues within the same peptide sequence) with 2 Da mass loss with confidence. SSH and intra-peptide disulfide were observed as the two most common thiol PTMs in this dataset.

3.3. *Alterations in β-cell global proteome by thapsigargin-induced ER stress*

ER stress has been reported as a potential mechanism contributing to pancreatic β-cell death in both type 1 diabetes and type 2 diabetes [45, 46]. However, the detailed proteome-wide response of pancreatic β-cells to ER stress has not been reported. Fig. 3A displays a substantial proteome response to Tg-induced ER stress at the protein expression level. Compared to control, 2945 out of 9342 proteins were either up- or down-regulated (adjusted p-value < 0.05) (Table S1). Based on Ingenuity Pathway Analysis (IPA) (Fig. 3B), the most significantly enriched canonical pathways include autophagy, protein ubiquitination pathway, unfolded protein response, EIF2 signaling, and tRNA charging. ER stress is well known for triggering autophagy [47] and the ubiquitin-proteasome system is also interconnected with ER stress regulation and autophagy [48]. Moreover, pathways related to β-cell

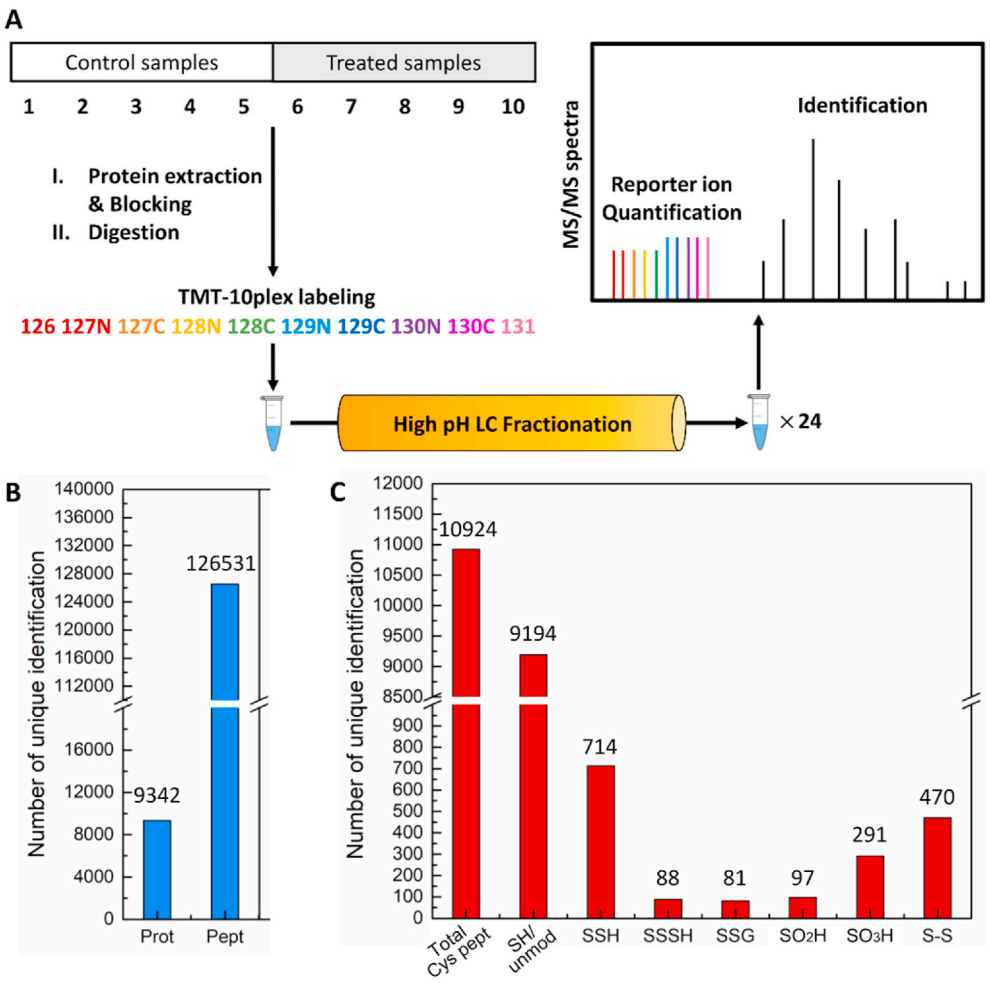

Fig. 2. Direct detection deep profiling workflow for simultaneous profiling of the global proteome and multiple thiol PTMs. (A) Sample preparation workflow comprised of 10-plex TMT labeling and high pH reversed phase LC fractionation. Pancreatic β-cells were treated with thapsigargin (Tg) to induce ER stress while cells without treatment were used as control. Proteins were extracted from 5 biological replicates of control and Tg-treated samples followed by HPE-IAM blocking and trypsin digestion. After TMT labeling, all samples were pooled and fractionated into 24 fractions. Intensities of reporter ions were quantified and compared across channels. (B) Global proteome coverage. (C) Coverage of cysteine-containing peptides, and different types of thiol PTM-containing peptides. Total Cys pept, total cysteine-containing peptides, SH/unmod, unmodified cysteine-containing peptides.

functions and cell fate were enriched as well, including the insulin secretion signaling pathway, G2/M DNA damage checkpoint regulation, sirtuin signaling pathway, etc. It was proposed that insulin secretion can be inhibited by dysregulation of ER stress signaling in the development of Type 2 diabetes mellitus [49], and possibly through loss of the insulin receptor [50]. Sirtuin as a NAD^+-dependent deacetylase is known to associate with oxidative stress, inflammation, and mitochondrial function [51]. It has been reported to be induced by ER stress and a contributor to ER stress-induced cellular damage [52], while Sirtuin may play a protective role in β cells and improve insulin resistance in insulin-sensitive tissues [51,53]. These enriched pathways suggest the presence of sophisticated regulatory networks in β cells.

Fig. 3C further highlights the expression changes of selected proteins in some of the top pathways. In response to Tg, increased protein abundances were observed in many known proteins involved in the unfolded protein response (UPR), including a number of classical ER stress response proteins such as activating transcription factor 6 (*Atf6*), activating transcription factor 4 (*Atf4*), DNA-damage inducible transcript 3 (*Ddit3*, aka. CHOP), endoplasmic reticulum chaperone BiP (GRP78), CCAAT/enhancer-binding protein β, γ (aka. C/EBP, *Cebpb*, *Cebpg*), and DnaJ heat shock proteins (*Dnaja3*, *Dnaja4*) [54]. The upregulation of these proteins indicated an enhanced protein folding activity by β-cells in response to the accumulation of unfolded or misfolded proteins due to ER stress induced by Tg. Moreover, increased active degradation activity of unwanted proteins was also observed, based on the upregulation of proteins (e.g. PAT complex subunit CCDC47) involved in ER-associated protein degradation (ERAD) (Table S1). Interestingly, expression of proteins mediating cell survival (e.g., apoptosis antagonizing transcription factor, *Aatf*) were also found to be upregulated (Table S1) [55]. These results suggest a balanced cell fate decision in β-cells in the presence of ER stress.

Significant upregulation of autophagy was also observed, including the upregulation of a number of autophagy-related proteins (ATGs) (Fig. 3C), which were previously reported to participate in autophagosome formation and are associated with UPR [56]. Sequestosome-1 (Sqstm1/p62) is another upregulated protein, which is reported to be involved in the degradation of misfolded proteins via selective autophagy [57]. EIF2 signaling was observed as upregulated in response to ER stress. Phosphorylated eukaryotic initiation factor 2 α subunit (EIF2α) sequesters EIF2β to inhibit general translation and protein synthesis during ER stress while upregulating translation of specific UPR mRNAs such as Atf4 [58]. In our results, components involved in forming the EIF2 ternary complex presented significantly higher protein abundances in the presence of ER stress induced by Tg (Fig. 3C), suggesting upregulation of EIF2 signaling at the protein translation level. Amino acid biosynthesis regulation (aka. tRNA charging) was another significantly upregulated pathway, covering tRNA synthetases using specific amino acids including Met, Leu, Trp, Val, Gly, Ala, and Cys (Fig. 3C). Interestingly, increased amino acid flux and tRNA charging during ER stress have been reported in β-cells despite attenuated protein synthesis, which is a general strategy to protect β cells from apoptosis [59].

Fig. 3D presents a graphical summary of the dataset based on IPA, which highlights some of the major biological themes identified and their associated relationships. Interestingly, IPA highlights a number of upstream regulators, including transcriptional regulators (e.g., FOXM1,

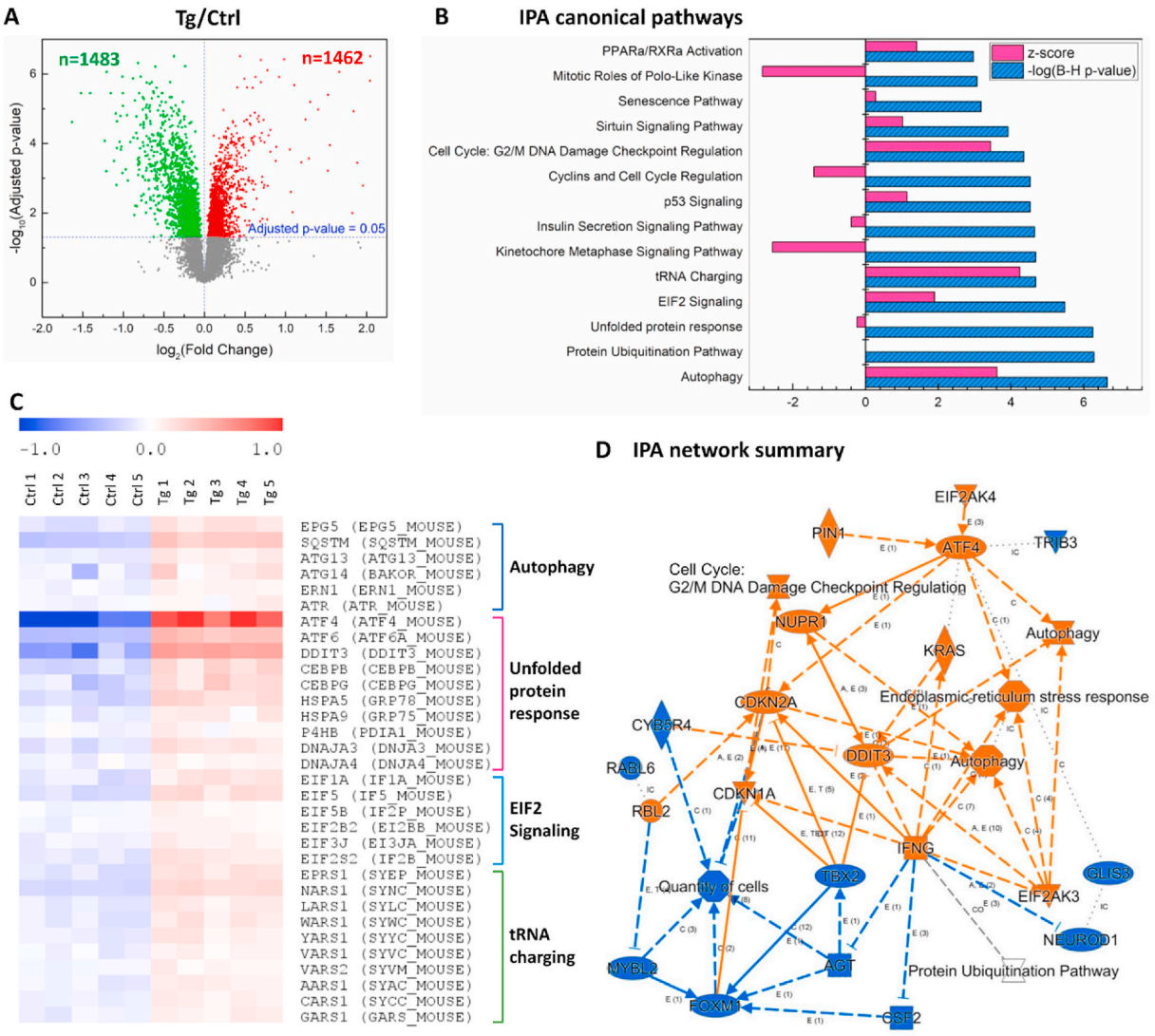

Fig. 3. Global proteome changes due to Thapsigargin-induced ER stress. (A) Volcano plot comparing protein expression levels in Tg-treated samples to control samples. Proteins with significant changes in abundance (adjusted p-value < 0.05) were indicated in red (up-regulated) or green (down-regulated). (B) Top canonical pathways from Ingenuity Pathway Analysis (IPA). The adjusted p-value indicated the significance of a given pathway being enriched with the observed genes/proteins. The z-score indicates the activation (z-score > 0) or inhibition (z-score < 0) of the given pathway based on the direction of abundance changes of associated proteins. (C) Heatmap of the differentially expressed proteins (adjusted p-value < 0.05) related to ER stress response. Relative abundances were log2 transformed. "Ctrl 1" – "Ctrl 5" are the replicates of control samples. "Tg 1" – "Tg 5" are the replicates of Tg-treated samples. Protein names are presented as abbreviation with Uniprot IDs. (D) Network summary from IPA. Proteins with significantly changed expression levels were used for the IPA functional analyses. (For interpretation of the references to colour in this figure legend, the reader is referred to the Web version of this article.)

NEUROD1) inferred from the observed abundance changes exhibited by their target proteins. FOXM1 is an important transcription factor that promotes β-cell proliferation through activation of genes necessary for cell cycle progression and insulin secretion [60,61] and is required for sustaining pancreatic β-cell mass in mice [62]. Previous studies have found that the NEUROD1 transcription factor is required for processes such as pancreatic development or insulin expression and mutations of this gene are known to cause type II diabetes [63,64]. The inhibition of these transcriptional regulators could be potential novel mechanisms involved in how pancreatic β-cells respond to ER stress. Down-regulation of FOXM1 or NEUROD1 pathways could result in reduced proliferative capacity, function, or insulin secretion, in an effort by the β-cell to manage ER stress and promote cell survival.

3.4. Detection of multiple types of thiol PTMs and their changes under ER stress

One of our interests was to identify redox-dependent post-translational regulation through different types of thiol PTMs in addition to translational regulation. In our dataset, 1730 out of 10,924 unique cysteine-containing peptides are modified with different forms of redox PTMs (Fig. 2C). We further aggregated these modified peptides to the Cys site level by summing reporter ion intensities of peptides with the same modifications on the same Cys sites. In total, 1506 Cys sites were quantified, carrying different types of modifications across samples. Due to the relatively large variation of the abundance data at the PTM level, we applied a relatively loose cutoff of p-value < 0.025 and adjusted p-value < 0.15 to identify thiol PTMs with significant changes. 129 modified Cys sites showed increased levels, while 102 Cys sites had decreased levels of modifications in response to Tg treatment (Fig. 4A). Consistent with previous reports, the majority of SSH-modified Cys sites

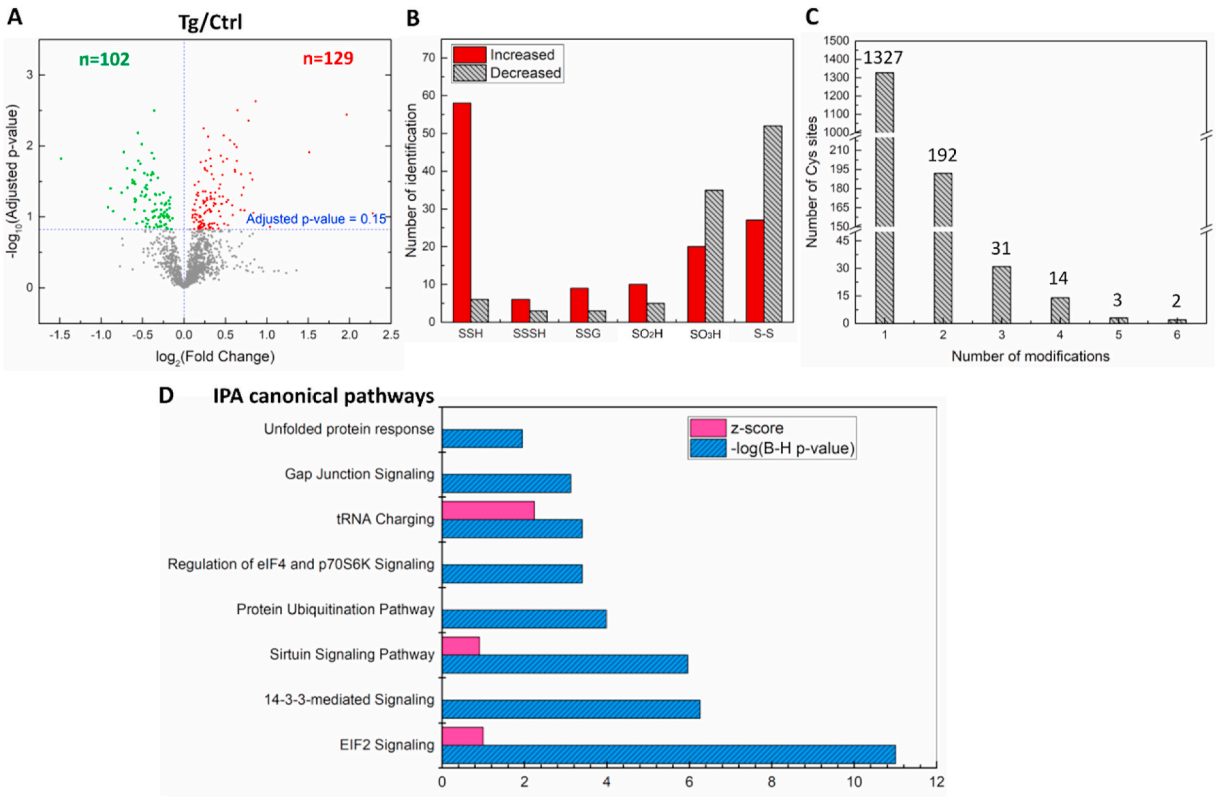

Fig. 4. Thiol modification changes due to Thapsigargin-induced ER stress. (A) Volcano plot comparing modification level of Cys sites in Tg-treated samples to control samples. Cys sites with significantly altered at modification level (p-value < 0.025 and adjusted p-value < 0.15) were indicated in red (increased level) or green (decreased level). (B) Number of identifications for each type of modification analyzed that exhibited significantly changed levels on Cys sites. (C) Histogram representing the distribution of the number of Cys sites observed with 1–6 forms of modifications. (D) Top canonical pathways from IPA. Cys sites with significantly altered PTM levels were used for the IPA functional analyses. (For interpretation of the references to colour in this figure legend, the reader is referred to the Web version of this article.)

displayed increased levels in Tg-treated samples (Fig. 4B), suggesting that the SSH modification was promoted in the presence of ER stress where more active H_2S and ROS production may occur [22]. Moreover, SSSH-modified sites displayed increased levels, following the same trend as SSH, despite the overall low number of observed SSSH-modifications. Additionally, >15% of the Cys sites were observed with more than one type of PTM with some of the sites containing 4–6 types of modifications on the same sites (Fig. 4C). IPA analysis of the proteins with significant changes at the PTM level revealed several enriched canonical pathways (Fig. 4D). Despite the small number of modified proteins in total (n = 231), several common pathways were identified at both the protein expression and PTM level, including EIF2 signaling, Sirtuin signaling pathway, protein ubiquitination pathway, tRNA charging, and unfolded protein response. Overall, the data suggest that many of these pathways are regulated at both translational and post-translational levels through redox PTMs. In some cases, changes in redox PTMs are clearly independent of changes in protein abundance. For example, ER stress response proteins including protein disulfide isomerase associated 3 (*Pdia3*), transitional endoplasmic reticulum ATPase (*Vcp*), eukaryotic translation elongation factor 2 (*Eef2*), and ER resident protein 29 (*Erp29*) showed decreased levels of thiol PTMs, although the changes in abundance of these proteins were either not significant or slightly increased in the Tg-treated condition compared to the controls (Table S3).

3.5. Complexity of multiform PTMs on the same Cys residues and their functional implications

Perhaps the most revealing data from this study is the observation of multiple types of modifications at the same Cys sites for different proteins (Table 1), representing a novel set of data reflecting the complexity of thiol PTMs. For example, Cys150 at the catalytic site of GAPDH is a well-established example of a redox-sensitive cysteine that can be altered, and impact enzymatic activities as mentioned in the introduction. On Cys150, we identified SSH, SSSH, SO_2H, SO_3H, SSG, as well as a disulfide with the neighboring Cys154. The diversity of modifications at this site suggests that GAPDH is sensitive to the changes in the oxidative environment, which in turn leads to subtle changes in protein activity. Among these modifications, increased levels of SSH and SSG were quantified in Tg-treated samples compared to control while the abundance of GAPDH was not significantly changed (Table S3). On the contrary, the levels of SO_2H, SO_3H, and disulfides were significantly decreased. Interestingly, we also observed a proteoform where Cys150 and Cys154 had SO_3H at the same time, suggesting that there are catalytically inactivated instances of GAPDH present in the cell.

Another example is the autophagic receptor protein Sqstm1/p62, which was observed as upregulated during ER stress. p62 is known to be controlled via PTMs, including phosphorylation, ubiquitination, and oxidation [65–67]. Cys105 and Cys113 are the two cysteines that tend to form a disulfide bond for oligomerization in oxidative stress conditions, promoting the formation of autophagosomes [67]. In our datasets, no Cys105- or Cys113-containing peptides were identified due to the limitation of trypsin digestion in this study. Instead, a variety of modifications were identified on three CXXC motifs of Sqstm1/p62 including Cys128 and Cys131, Cys142 and Cys145, Cys151 and Cys154 (Fig. 5; Table S3), where disulfides were found on all three motifs. With correction by protein abundance fold-change, Cys128 and Cys131, Cys142 and Cys145 showed significantly higher levels of disulfide formation in the Tg-treated samples. Furthermore, SSH on Cys128 and SSH and SO_2H on Cys131 were identified, suggesting that this motif was

Table 1
Proteins with Cys sites bearing multiple types of PTM types (n ≥ 4).

Protein ID	Protein description	Representative seq	Cys Site	# of PTM types	Detected PTMs
1433T_MOUSE	14-3-3 protein theta	DNLTLWTSDSAGEEC̲DAAEGAEN	237	4	SO_2H, SO_3H, SSG, SSH
EF1A1_MOUSE	Elongation factor 1-alpha 1	PMC̲VESFSDYPPLGR	411	4	SO_3H, SSG, SSH, SSSH
ERH_MOUSE	Enhancer of rudimentary homolog	TYADYESVNEC̲MEGVCK	28	4	S–S, SO_2H, SSH, SSSH
G3P_MOUSE	Glyceraldehyde-3-phosphate dehydrogenase	IVSNASC̲TTNC̲LAPLAK	150	6	S–S, SO_2H, SO_3H, SSG, SSH, SSSH
		IVSNASCTTNC̲LAPLAK	154	6	S–S, SO_2H, SO_3H, SSG, SSH, SSSH
GDIB_MOUSE	Rab GDP dissociation inhibitor beta	TDDYLDQPCC̲ETINR	203	4	SO_3H, SSH, SSSH, S–S
MDHC_MOUSE	Malate dehydrogenase, cytoplasmic	ENFSC̲LTR	154	4	SO_2H, SO_3H, SSG, SSH
MDHM_MOUSE	Malate dehydrogenase, mitochondrial	GYLGPEQLPDC̲LKGCDVVV	89	4	S–S, SO_2H, SO_3H, SSH
		GYLGPEQLPDCLKGC̲DVVV	93	5	SO_2H, SO_3H, SSG, SSH, S–S
PARK7_MOUSE	Parkinson disease protein 7 homolog	VTVAGLAGKDPVQC̲SR	46	4	SO_2H, SO_3H, SSG, SSH
PGAM1_MOUSE	Phosphoglycerate mutase 1	YADLTEDQLPSC̲ESLK	153	4	SO_2H, SO_3H, SSG, SSH
PGK1_MOUSE	Phosphoglycerate kinase 1	TGQATVASGIPAGWMGLDC̲GTESSK	316	4	SO_2H, SO_3H, SSH, SSSH
TBA1A_MOUSE	Tubulin alpha-1A chain	AYHEQLSVAEITNAC̲FEPANQMVKCDPR	295	5	S–S, SO_2H, SO_3H, SSH, SSSH
TBA1B_MOUSE	Tubulin alpha-1B chain	SIQFVDWC̲PTGFK	347	4	SO_2H, SO_3H, SSH, SSSH
TBB1_MOUSE	Tubulin beta-1 chain	ENTDACFC̲IDNEALYDICFR	201	4	SO_3H, S–S, SSSH, SSH
TBB2A_MOUSE	Tubulin beta-2A chain	LTTPTYGDLNHLVSATMSGVTTC̲LR	239	5	SO_2H, SO_3H, SSG, SSH, SSSH
TBB4A_MOUSE	Tubulin beta-4A chain	EIVHLQAGQC̲GNQIGAKF	12	4	SO_2H, SO_3H, SSG, SSH
TERA_MOUSE	Transitional endoplasmic reticulum ATPase	IHCEGEPIKREDEEESLNEVGYDDIGGC̲R	209	4	SO_2H, SO_3H, SSH, S–S
UBA1_MOUSE	Ubiquitin-like modifier-activating enzyme 1	DNPGVVTC̲LDEAR	234	4	SO_2H, SO_3H, SSH, SSSH

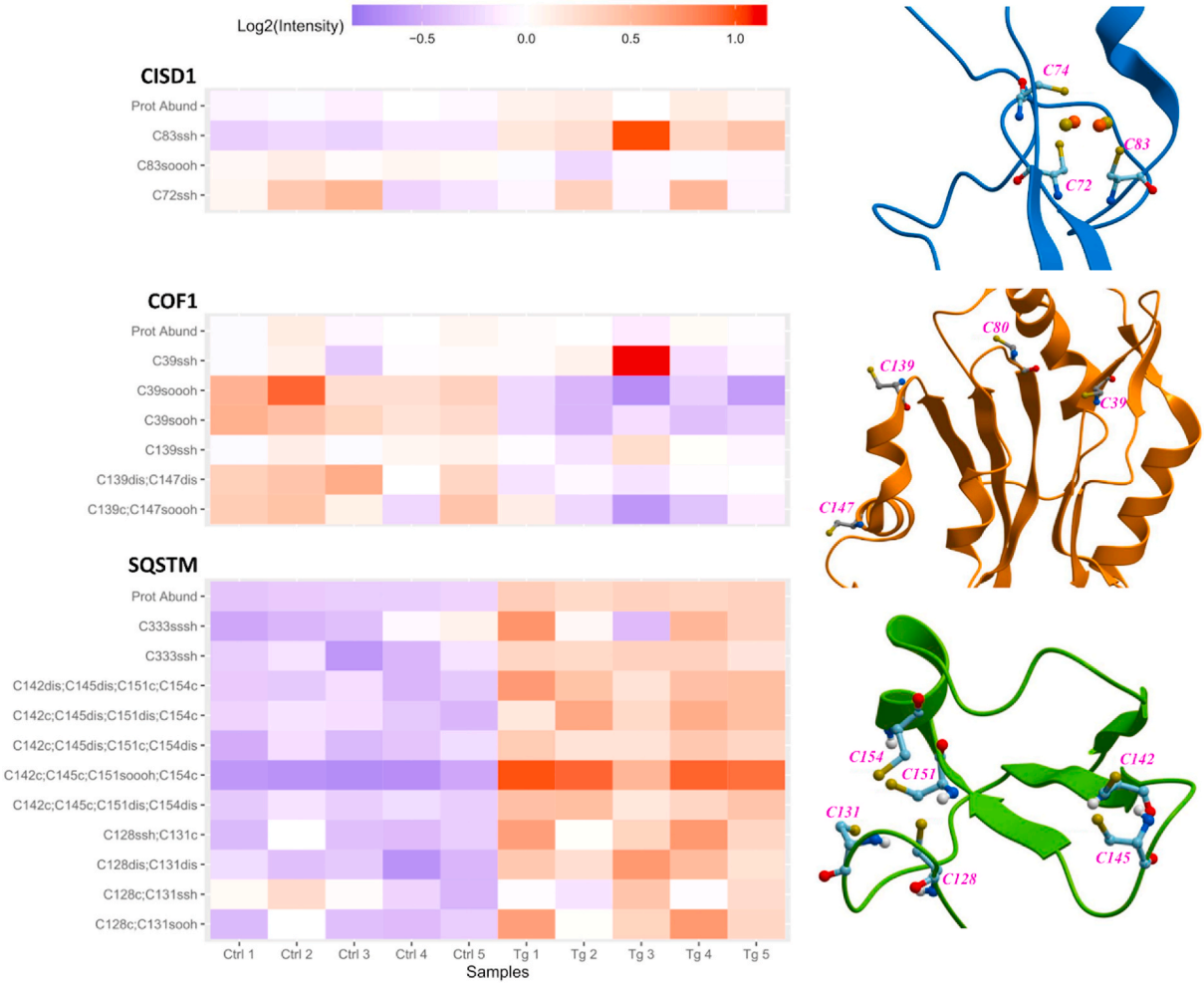

Fig. 5. Levels of multiple types of modifications on Cys sites of CISD1, COF1 and SQSTM/p62 and their structures (PDB: 3REE, 6VAO, 5YP7) [94–96] highlighting Cys locations. CISD1: Cys72, Cys74, and Cys83 (identified in our study) are shown to illustrate their close proximity to each other and the [2Fe–2S] cluster. Orange spheres represent Iron atoms while yellow spheres represent the sulfur atoms. COF1: Cys39, 80 (shown here to emphasize proximity with Cys39), 139, and 147 are highlighted in the structure. SQSTM: Cys sites 128, 131, 142, 145, 151, and 154 are illustrated in structure. The heatmaps on the left display abundance changes at both the protein level and the PTM level for different Cys sites. Dis: disulfide. (For interpretation of the references to colour in this figure legend, the reader is referred to the Web version of this article.)

sensitive to multiple redox signals.

Another major class of proteins observed with multiple types of redox PTMs are cytoskeletal components. We uncovered numerous sites on both alpha- and beta-tubulin (Table S3), in agreement with a proposed concept of redox-dependent regulation of cytoskeletal dynamics as was described for neuronal cells in a previous review [68]. Actin is another type of cytoskeletal protein that has many interacting proteins including those that modulate their polymerization, such as the redox regulated protein Cofilin-1 (COF1) [69,70]. A previous report investigating an isoform of Cofilin-1, named Cofilin-2, identified Cys39 as a critical residue for the formation of a disulfide with Cys80 (also illustrated for Cofilin-1 in Fig. 5), where the phosphorylation status of the protein impacts whether this disulfide forms, leading to formation of fibrillar aggregates [71]. Molecular dynamic simulations from this work showed that Cys39 is more easily oxidized when Cofilin-2 is phosphorylated, leading to formation of a disulfide. Intriguingly, the same study found that WT Cofilin-2 treated with H_2O_2 showed no signs of oxidation, however a phosphomimetic of the same protein treated with H_2O_2 resulted in SO_3H or thiosulfonic acid (S_2O_2H) at Cys39, which is believed to be a degradation product of a former disulfide bridge [71]. In contrast, our data shows significant down-regulation of SO_2H or SO_3H at Cys39 following ER stress (Fig. 5), suggesting that more disulfides could be formed following ER stress, however we did not observe any Cys39-80 disulfides; presumably due to the limitation of shotgun proteomics in identifying disulfides.

Beyond identification of proteins associated with metabolism and cytoskeletal structure, proteins with Cys modifications are also involved in an array of other biological processes. The protein CDGSH iron-sulfur domain-containing protein 1 (CISD1, aka. MitoNEET) is putative redox sensing protein with several cysteine residues in its metal binding (iron) cluster [72]. Among these is Cys83, which forms a disulfide with either Cys72 or 74 of another protomer, resulting in the formation of a homodimer [73]. CISD1 has been found to interact with the insulin regulator glutamate dehydrogenase 1 (GDH1) via an intermolecular disulfide bond between Cys74 of MitoNEET and Cys319 of GDH1 [73]. In our study, we found that Cys83 contained a SO_3H modification (Fig. 5, Table S3), which could prevent both homodimerization of MitoNEET as well as subsequent disulfide formation with GDH1, which is needed to enhance its activity. Interestingly, the SO_3H modification was downregulated following induction of ER stress in our data, which may mean that more MitoNEET homodimers are present and GDH1 activity could be upregulated. Further work is needed to test this theory as well as determine the effects of the SO_3H modification. The ubiquitin C-terminal hydrolase L1 (UCHL1) is an abundant deubiquitinase in neurons and β-cells and is emerging as a biomarker of β-cell destruction [74]. A deficiency in UCHL1 function leads to an increase in toxic protein aggregates and is implicated in mechanisms that cause neurodegenerative diseases as well as Type II diabetes [75,76]. It was found in a later study in myeloma cells that Cys220, found within the essential CKAA motif, is required for promoting mTOR-AKT signaling and interacts with translation initiation factors to promote assembly of the initiation complex [77]. In our dataset, Cys220 exhibited a minor increase in SSH and moderate decrease in SO_3H following induction of ER stress (Fig. S1, Table S3). The effect of these redox PTMs on the function of UCHL1 are not known, however another report found that SNO at Cys220 leads to its instability [78], emphasizing the importance of redox PTMs in UCHL1's function.

4. Discussion

The high reactivity of protein cysteine thiols and the complex redox microenvironments in which they exist make the redox sensitive Cys residues amenable to form an array of redox PTMs, each potentially leading to different biological effects on a protein. The complex and dynamic nature of redox PTMs makes their precise and quantitative characterization a daunting challenge in redox biology. Current knowledge about thiol redox PTMs and their associated proteins has stemmed from studies that investigated specific forms of cysteine oxidation (through chemo-specific probes or their selective reduction) or broadly (block free thiols, reduce all reversibly oxidized thiols, then enrichment or labeling of nascent free thiols). The SSG, SOH, SNO, or total reversible cysteine oxidation profile can be ascertained using indirect methods [79], however other modifications such as SO_2H or SO_3H are more challenging to identify using the same approach since they are typically irreversibly oxidized. To overcome this problem, development of specific probes that select for SO_2H have been reported [80], but SO_3H remains difficult to probe. Together, these methods have greatly improved our understanding of redox PTMs; however, knowledge regarding the landscape of multiple types of redox PTMs in a given biological system and their response to perturbations is still very limited. Moreover, profiling for one type of redox PTM provides an incomplete account of redox regulation through multiple types of PTMs that a protein and cysteine site will encounter, which may interfere with how redox regulation of a protein or pathway is interpreted. Therefore, the redox biology field requires new techniques that can investigate multiple types of thiol oxidation simultaneously to gain a more comprehensive view into the diversity of redox PTMs at a given site.

4.1. Advantages and limitations of the direct detection assay for thiol PTMs

The present direct detection assay enables simultaneous measurements of both protein abundances and multiple types of thiol PTMs through preserving stable thiol PTMs with a relatively mild alkylation reagent, HPE-IAM, for blocking reactive thiols and a deep proteome profiling workflow. The ability of this method to uncover multiple types of thiol PTMs in a single experimentmakes it complementary to most other thiol redox proteomics approaches, which typically focus on one type of thiol PTM through specific enrichment strategy. The multiform PTMs detected on key proteins provide a unique level of information on the complexity of thiol PTMs and their regulation on key functional cysteine sites that are typically unavailable in other indirect profiling studies. We should also note that this direct detection strategy is not limited to thiol PTMs since all stable PTMs should be identifiable with proper sample preparation for preservation of PTMs of interest. The ability to perform integrated dynamic measurements of both protein abundances and individual PTMs in this workflow is another significant advantage for delineating translational and post-translational changes and for investigating potential crosstalk between different types of PTMs (e.g. redox vs. phosphorylation) on protein structure and function.

While the current direct detection strategy holds potential for uncovering multiform thiol PTMs, there are several caveats associated with this method. First, the overall coverage of Cys sites with PTMs is still relatively low compared to those achievable with specific enrichment strategies [81,82]. The relatively low coverage of modified Cys sites is somewhat anticipated given that no enrichment strategy is applied in this workflow. The current dataset only observed 275 proteins with significant changes in thiol PTMs, which is insufficient to provide a broad view of the redox-dependent pathways involved in ER stress regulation. Consequently, the current indirect approaches are more useful as tools to obtain a global picture of the redox proteome [81–83]. Second, several thiol PTMs such as SNO or SOH are known for their instability and reactivity, leading to their conversion of other redox PTMs such as SSG [84,85], or in the case of SOH, progression to SO_2H and SO_3H [8]. The alkylation-based stabilization of SSSH or higher order of hydropolysulfides also remains challenging [31]. Direct detection of such labile modifications would be challenging. Third, due to the nature of the tripeptide glutathione, direct identification of SSG also presents its own challenge, as fragmentation of peptides with SSG during LC-MS/MS analysis can result in complex spectra [86]. Since SSG contributes a mass of 305.0682 Da to cysteine, glutathione itself will be fragmented like a peptide, leading to neutral loss. As an alternative and complementary

approach, indirect methods that derivatize specific PTMs have proven valuable for detection of these labile and challenging modifications [79,87–89]. Fourth, despite the known relative abundance of inter-chain disulfides in proteins, detection of such disulfides at proteome level has been a bioinformatics challenge [90,91]. While we did not attempt to cover interchain disulfide in this work, such identifications are certainly worth additional efforts. Finally, the general stability of thiol PTMs and their interconversion including disulfide reshuffling both in situ and during sample processing should be taken into consideration for data interpretation. For instance, it is established that disulfide oxidation can result in many forms of thiol PTMs such SOH, SO_2H, SO_3H, as well as SSG [7,92]. Moreover, disulfide reshuffling can occur during sample processing due to the alkaline pH, which may introduce disulfide artifacts via unblocked free thiols [91]; therefore, the initial efficient blocking step of free thiols by alkylation is critical to prevent such artifacts. Such complexity of interconversion of thiol PTMs presents a further challenge in interpreting the significance of observed thiol PTMs.

4.2. Challenges in interpreting the potential significance of thiol PTMs

With all the data generated from single PTM or multiple PTM profiling experiments, identifying the biological significance of the PTMs on a protein (if they are not yet known) is always a challenge. This is especially true when multiple types of PTMs are observed at the same site, which may even have opposing effects on a protein (i.e. enhanced or reduced function). It is unclear how different types of PTMs are regulated at the specific Cys sites such as GAPDH Cys150, whether the specific PTM was converted from another PTM such as SOH, and which modification type has more significant functional impact. Analytical advances are still clearly needed to quantify different types of modifications in a stoichiometric manner [93]. This is essential for grasping how the distribution of different PTMs with a common Cys site influence underlying protein functions and biological processes. Currently, genetic and biochemical methods remain the most widely used approaches to understand the biological relevance of a site and a specific PTM. Genetic follow-up experiments typically incorporate site directed mutagenesis of a Cys site or knockdown of the protein to see if there is any effect in a biological system, while biochemical methods can provide insight into how a PTM may affect a protein's specific function. In this way, the effects of redox PTMs can be characterized to determine what proportion of protein identified in a direct detection assay is active. Modeling the different types of PTMs observed at the same Cys site may provide insight into their effects on protein structure. Molecular dynamic simulations of these modifications may provide clues as to how a redox PTM may inhibit or enhance a protein's function. The combined efforts of direct and indirect proteomic approaches along with in-depth genetic or biochemical studies can uncover significant redox-regulated Cys sites to guide selection of proteins for future studies involved in drug design or biomarker evaluation.

In summary, the direct detection workflow enables simultaneous profiling of the global proteome and the thiol redox proteome with coverage of multiple types of thiol PTMs as demonstrated in mouse pancreatic β-cells under ER stress. The results not only reveal distinct translational and posttranslational regulation in response to ER stress, but more importantly uncover the complexity of multiple types of thiol redox PTMs, which often occur on the same Cys residues. The observed complexity of thiol PTMs further highlights the challenge in the characterization and interpretation of protein thiol modifications in redox biology.

Funding statement

This work was supported in part by NIH grants R01 GM125968 (to M.X.), R01 DK122160 (to W.Q.), and R01 HL139335 (to W.Q.).

Declaration of competing interest

The authors declare no conflict of interests.

Acknowledgements

The experimental work described herein was performed in the Environmental Molecular Sciences Laboratory, Pacific Northwest National Laboratory, a national scientific user facility sponsored by the Department of Energy under Contract DE-AC05-76RL0 1830.

Appendix A. Supplementary data

Supplementary data to this article can be found online at https://doi.org/10.1016/j.redox.2021.102111.

References

[1] C.E. Paulsen, K.S. Carroll, Cysteine-mediated redox signaling: chemistry, biology, and tools for discovery, Chem. Rev. 113 (7) (2013) 4633–4679.
[2] J.M. Held, B.W. Gibson, Regulatory control or oxidative damage? Proteomic approaches to interrogate the role of cysteine oxidation status in biological processes *, Mol. Cell. Proteomics 11 (4) (2012).
[3] H.J. Forman, J.M. Fukuto, M. Torres, Redox signaling: thiol chemistry defines which reactive oxygen and nitrogen species can act as second messengers, Am. J. Physiol. Cell Physiol. 287 (2) (2004) C246–C256.
[4] C.C. Winterbourn, M.B. Hampton, Thiol chemistry and specificity in redox signaling, Free Radic. Biol. Med. 45 (5) (2008) 549–561.
[5] M. Benhar, Oxidants, antioxidants and thiol redox switches in the control of regulated cell death pathways, Antioxidants 9 (4) (2020).
[6] Y.M. Go, J.D. Chandler, D.P. Jones, The cysteine proteome, Free Radic. Biol. Med. 84 (2015) 227–245.
[7] L. Carroll, S. Jiang, J. Irnstorfer, S. Beneyto, M.T. Ignasiak, L.M. Rasmussen, A. Rogowska-Wrzesinska, M.J. Davies, Oxidant-induced glutathionylation at protein disulfide bonds, Free Radic. Biol. Med. 160 (2020) 513–525.
[8] M. Lo Conte, K.S. Carroll, The redox biochemistry of protein sulfenylation and sulfinylation, J. Biol. Chem. 288 (37) (2013) 26480–26488.
[9] H.A. Woo, W. Jeong, T.S. Chang, K.J. Park, S.J. Park, J.S. Yang, S.G. Rhee, Reduction of cysteine sulfinic acid by sulfiredoxin is specific to 2-cys peroxiredoxins, J. Biol. Chem. 280 (5) (2005) 3125–3128.
[10] M.B. Feeney, C. Schöneich, Tyrosine modifications in aging, Antioxidants Redox Signal. 17 (11) (2012) 1571–1579.
[11] M. Ehrenshaft, L.J. Deterding, R.P. Mason, Tripping up Trp: modification of protein tryptophan residues by reactive oxygen species, modes of detection, and biological consequences, Free Radic. Biol. Med. 89 (2015) 220–228.
[12] A. Bachi, I. Dalle-Donne, A. Scaloni, Redox proteomics: chemical principles, methodological approaches and biological/biomedical promises, Chem. Rev. 113 (1) (2013) 596–698.
[13] X. Zhang, M.E. Monroe, B. Chen, M.H. Chin, T.H. Heibeck, A.A. Schepmoes, F. Yang, B.O. Petritis, D.G. Camp 2nd, J.G. Pounds, J.M. Jacobs, D.J. Smith, D. J. Bigelow, R.D. Smith, W.J. Qian, Endogenous 3,4-dihydroxyphenylalanine and dopaquinone modifications on protein tyrosine: links to mitochondrially derived oxidative stress via hydroxyl radical, Mol. Cell. Proteomics 9 (6) (2010) 1199–1208.
[14] M.-A. Tossounian, B. Zhang, I. Gout, The writers, readers, and erasers in redox regulation of GAPDH, Antioxidants 9 (12) (2020) 1288.
[15] T. Hildebrandt, J. Knuesting, C. Berndt, B. Morgan, R. Scheibe, Cytosolic thiol switches regulating basic cellular functions: GAPDH as an information hub? Biol. Chem. 396 (5) (2015) 523–537.
[16] M. Zaffagnini, S. Morisse, M. Bedhomme, C.H. Marchand, M. Festa, N. Rouhier, S. D. Lemaire, P. Trost, Mechanisms of nitrosylation and denitrosylation of cytoplasmic glyceraldehyde-3-phosphate dehydrogenase from Arabidopsis thaliana, J. Biol. Chem. 288 (31) (2013) 22777–22789.
[17] K.V. Barinova, M.V. Serebryakova, V.I. Muronetz, E.V. Schmalhausen, S-glutathionylation of glyceraldehyde-3-phosphate dehydrogenase induces formation of C150-C154 intrasubunit disulfide bond in the active site of the enzyme, Biochim. Biophys. Acta Gen. Subj. 1861 (12) (2017) 3167–3177.
[18] K.V. Barinova, M.V. Serebryakova, M.A. Eldarov, A.A. Kulikova, V.A. Mitkevich, V. I. Muronetz, E.V. Schmalhausen, S-glutathionylation of human glyceraldehyde-3-phosphate dehydrogenase and possible role of Cys152-Cys156 disulfide bridge in the active site of the protein, Biochim. Biophys. Acta Gen. Subj. 1864 (6) (2020) 129560.
[19] X. Gao, L. Li, M. Parisien, J. Wu, I. Bederman, Z. Gao, d. krokowski, S. M. Chirieleison, D.W. Abbott, B. Wang, P. Arvan, M. Cameron, M. Chance, B. B. Willard, M. Hatzoglou, Discovery of a redox thiol switch: implications for cellular energy metabolism, Molecular & Cellular Proteomics 19 (5) (2020) 852–870.
[20] D. Su, M.J. Gaffrey, J. Guo, K.E. Hatchell, R.K. Chu, T.R.W. Clauss, J.T. Aldrich, S. Wu, S. Purvine, D.G. Camp, R.D. Smith, B.D. Thrall, W.-J. Qian, Proteomic identification and quantification of S-glutathionylation in mouse macrophages

using resin-assisted enrichment and isobaric labeling, Free Radic. Biol. Med. 67 (2014) 460–470.
[21] S.R. Jaffrey, H. Erdjument-Bromage, C.D. Ferris, P. Tempst, S.H. Snyder, Protein S-nitrosylation: a physiological signal for neuronal nitric oxide, Nat. Cell Biol. 3 (2) (2001) 193–197.
[22] X.-H. Gao, D. Krokowski, B.-J. Guan, I. Bederman, M. Majumder, M. Parisien, L. Diatchenko, O. Kabil, B. Willard, R. Banerjee, B. Wang, G. Bebek, C.R. Evans, P. L. Fox, S.L. Gerson, C.L. Hoppel, M. Liu, P. Arvan, M. Hatzoglou, Quantitative H2S-mediated protein sulfhydration reveals metabolic reprogramming during the integrated stress response, eLife 4 (2015), e10067.
[23] M.T. Forrester, J.W. Thompson, M.W. Foster, L. Nogueira, M.A. Moseley, J. S. Stamler, Proteomic analysis of S-nitrosylation and denitrosylation by resin-assisted capture, Nat. Biotechnol. 27 (6) (2009) 557–559.
[24] D. Su, A.K. Shukla, B. Chen, J.-S. Kim, E. Nakayasu, Y. Qu, U. Aryal, K. Weitz, T.R. W. Clauss, M.E. Monroe, D.G. Camp Ii, D.J. Bigelow, R.D. Smith, R.N. Kulkarni, W.-J. Qian, Quantitative site-specific reactivity profiling of S-nitrosylation in mouse skeletal muscle using cysteinyl peptide enrichment coupled with mass spectrometry, Free Radic. Biol. Med. 57 (2013) 68–78.
[25] L.I. Leichert, F. Gehrke, H.V. Gudiseva, T. Blackwell, M. Ilbert, A.K. Walker, J. R. Strahler, P.C. Andrews, U. Jakob, Quantifying changes in the thiol redox proteome upon oxidative stress in vivo, Proc. Natl. Acad. Sci. U. S. A. 105 (24) (2008) 8197–8202.
[26] C.I. Murray, H. Uhrigshardt, R.N. O'Meally, R.N. Cole, J.E. Van Eyk, Identification and quantification of S-nitrosylation by cysteine reactive tandem mass tag switch assay, Mol. Cell. Proteomics : MCP 11 (2) (2012). M111 013441.
[27] Z. Qu, F. Meng, R.D. Bomgarden, R.I. Viner, J. Li, J.C. Rogers, J. Cheng, C. M. Greenlief, J. Cui, D.B. Lubahn, G.Y. Sun, Z. Gu, Proteomic quantification and site-mapping of S-nitrosylated proteins using isobaric iodoTMT reagents, J. Proteome Res. 13 (7) (2014) 3200–3211.
[28] S.R. Jaffrey, H. Erdjument-Bromage, C.D. Ferris, P. Tempst, S.H. Snyder, Protein S-nitrosylation: a physiological signal for neuronal nitric oxide, Nat. Cell Biol. 3 (2) (2001) 193–197.
[29] J. Guo, M.J. Gaffrey, D. Su, T. Liu, D.G. Camp, R.D. Smith, W.-J. Qian, Resin-assisted enrichment of thiols as a general strategy for proteomic profiling of cysteine-based reversible modifications, Nat. Protoc. 9 (1) (2014) 64–75.
[30] L. Fu, K. Liu, J. He, C. Tian, X. Yu, J. Yang, Direct Proteomic Mapping of Cysteine Persulfidation, Antioxidants & Redox Signaling, 2019.
[31] V. Bogdándi, T. Ida, T.R. Sutton, C. Bianco, T. Ditrói, G. Koster, H.A. Henthorn, M. Minnion, J.P. Toscano, A. van der Vliet, M.D. Pluth, M. Feelisch, J.M. Fukuto, T. Akaike, P. Nagy, Speciation of reactive sulfur species and their reactions with alkylating agents: do we have any clue about what is present inside the cell? Br. J. Pharmacol. 176 (4) (2018) 646–670.
[32] T. Akaike, T. Ida, F.-Y. Wei, M. Nishida, Y. Kumagai, M.M. Alam, H. Ihara, T. Sawa, T. Matsunaga, S. Kasamatsu, A. Nishimura, M. Morita, K. Tomizawa, A. Nishimura, S. Watanabe, K. Inaba, H. Shima, N. Tanuma, M. Jung, S. Fujii, Y. Watanabe, M. Ohmuraya, P. Nagy, M. Feelisch, J.M. Fukuto, H. Motohashi, Cysteinyl-tRNA synthetase governs cysteine polysulfidation and mitochondrial bioenergetics, Nat. Commun. 8 (1) (2017) 1177.
[33] J. Duan, V.K. Kodali, M.J. Gaffrey, J. Guo, R.K. Chu, D.G. Camp, R.D. Smith, B. D. Thrall, W.-J. Qian, Quantitative profiling of protein S-glutathionylation reveals redox-dependent regulation of macrophage function during nanoparticle-induced oxidative stress, ACS Nano 10 (1) (2016) 524–538.
[34] S. Longen, F. Richter, Y. Köhler, I. Wittig, K.-F. Beck, J. Pfeilschifter, Quantitative persulfide site identification (qPerS-SID) reveals protein targets of H2S releasing donors in mammalian cells, Sci. Rep. 6 (2016), 29808-29808.
[35] J. Duan, T. Zhang, M.J. Gaffrey, K.K. Weitz, R.J. Moore, X. Li, M. Xian, B.D. Thrall, W.-J. Qian, Stochiometric quantification of the thiol redox proteome of macrophages reveals subcellular compartmentalization and susceptibility to oxidative perturbations, Redox Biol 36 (2020) 101649.
[36] M.J. Gaffrey, N.J. Day, X. Li, W.J. Qian, Resin-assisted capture coupled with isobaric tandem mass tag labeling for multiplexed quantification of protein thiol oxidation, JoVE : JoVE 172 (2021).
[37] J. Duan, V.K. Kodali, M.J. Gaffrey, J. Guo, R.K. Chu, D.G. Camp, R.D. Smith, B. D. Thrall, W.J. Qian, Quantitative profiling of protein S-glutathionylation reveals redox-dependent regulation of macrophage function during nanoparticle-induced oxidative stress, ACS Nano 10 (1) (2016) 524–538.
[38] S. Kim, P.A. Pevzner, MS-GF plus makes progress towards a universal database search tool for proteomics, Nat. Commun. 5 (2014).
[39] Y. Benjamini, Y. Hochberg, Controlling the false discovery rate: a practical and powerful approach to multiple testing, J. Roy. Stat. Soc. B 57 (1995) 289–300.
[40] Y. Benjamini, D.J.A.o.s. Yekutieli, The Control of the False Discovery Rate in Multiple Testing under Dependency, 2001, pp. 1165–1188.
[41] A. Kramer, J. Green, J. Pollard Jr., S. Tugendreich, Causal analysis approaches in ingenuity pathway analysis, Bioinformatics 30 (4) (2014) 523–530.
[42] A.M. Evangelista, M.J. Kohr, E. Murphy, S-nitrosylation, specificity, occupancy, and interaction with other post-translational modifications, Antioxidants Redox Signal. 19 (11) (2013) 1209–1219.
[43] L.B. Poole, P.A. Karplus, A. Claiborne, Protein sulfenic acids in redox signaling, Annu. Rev. Pharmacol. Toxicol. 44 (2004) 325–347.
[44] H.A. Hamid, A. Tanaka, T. Ida, A. Nishimura, T. Matsunaga, S. Fujii, M. Morita, T. Sawa, J.M. Fukuto, P. Nagy, R. Tsutsumi, H. Motohashi, H. Ihara, T. Akaike, Polysulfide stabilization by tyrosine and hydroxyphenyl-containing derivatives that is important for a reactive sulfur metabolomics analysis, Redox biology 21 (2019), 101096-101096.
[45] F. Brozzi, D.L. Eizirik, ER stress and the decline and fall of pancreatic beta cells in type 1 diabetes, Ups, J. Med. Sci. 121 (2) (2016) 133–139.
[46] P. Marchetti, M. Bugliani, R. Lupi, L. Marselli, M. Masini, U. Boggi, F. Filipponi, G. C. Weir, D.L. Eizirik, M. Cnop, The endoplasmic reticulum in pancreatic beta cells of type 2 diabetes patients, Diabetologia 50 (12) (2007) 2486–2494.
[47] T. Yorimitsu, U. Nair, Z. Yang, D.J. Klionsky, Endoplasmic reticulum stress triggers autophagy, J. Biol. Chem. 281 (40) (2006) 30299–30304.
[48] W.X. Ding, H.M. Ni, W. Gao, T. Yoshimori, D.B. Stolz, D. Ron, X.M. Yin, Linking of autophagy to ubiquitin-proteasome system is important for the regulation of endoplasmic reticulum stress and cell viability, Am. J. Pathol. 171 (2) (2007) 513–524.
[49] C. Berry, M. Lal, B.K. Binukumar, Crosstalk between the unfolded protein response, MicroRNAs, and insulin signaling pathways: in search of biomarkers for the diagnosis and treatment of type 2 diabetes, Front. Endocrinol. 9 (2018), 210-210.
[50] M. Brown, S. Dainty, N. Strudwick, A.D. Mihai, J.N. Watson, R. Dendooven, A. W. Paton, J.C. Paton, M. Schröder, Endoplasmic reticulum stress causes insulin resistance by inhibiting delivery of newly synthesized insulin receptors to the cell surface, Mol. Biol. Cell 31 (23) (2020) 2597–2629.
[51] M. Kitada, Y. Ogura, I. Monno, D. Koya, Sirtuins and type 2 diabetes: role in inflammation, oxidative stress, and mitochondrial function, Front. Endocrinol. 10 (187) (2019).
[52] T. Koga, M.A. Suico, S. Shimasaki, E. Watanabe, Y. Kai, K. Koyama, K. Omachi, S. Morino-Koga, T. Sato, T. Shuto, K. Mori, S. Hino, M. Nakao, H. Kai, Endoplasmic reticulum (ER) stress induces sirtuin 1 (SIRT1) expression via the PI3K-Akt-GSK3β signaling pathway and promotes hepatocellular injury, J. Biol. Chem. 290 (51) (2015) 30366–30374.
[53] J.-H. Lee, M.-Y. Song, E.-K. Song, E.-K. Kim, W.S. Moon, M.-K. Han, J.-W. Park, K.-B. Kwon, B.-H. Park, Overexpression of SIRT1 protects pancreatic beta-cells against cytokine toxicity by suppressing the nuclear factor-kappaB signaling pathway, Diabetes 58 (2) (2009) 344–351.
[54] D. Ron, P. Walter, Signal integration in the endoplasmic reticulum unfolded protein response, Nat. Rev. Mol. Cell Biol. 8 (7) (2007) 519–529.
[55] S. Ishigaki, S.G. Fonseca, C.M. Oslowski, A. Jurczyk, J.R. Shearstone, L.J. Zhu, M. A. Permutt, D.L. Greiner, R. Bortell, F. Urano, AATF mediates an antiapoptotic effect of the unfolded protein response through transcriptional regulation of AKT1, Cell Death Differ. 17 (5) (2010) 774–786.
[56] M. Luhr, M.L. Torgersen, P. Szalai, A. Hashim, A. Brech, J. Staerk, N. Engedal, The kinase PERK and the transcription factor ATF4 play distinct and essential roles in autophagy resulting from tunicamycin-induced ER stress, J. Biol. Chem. 294 (20) (2019) 8197–8217.
[57] C. Kraft, M. Peter, K. Hofmann, Selective autophagy: ubiquitin-mediated recognition and beyond, Nat. Cell Biol. 12 (9) (2010) 836–841.
[58] K.M. Vattem, R.C. Wek, Reinitiation involving upstream ORFs regulates ATF4 mRNA translation in mammalian cells, Proc. Natl. Acad. Sci. U. S. A 101 (31) (2004) 11269.
[59] D. Krokowski, J. Han, M. Saikia, M. Majumder, C.L. Yuan, B.-J. Guan, E. Bevilacqua, O. Bussolati, S. Bröer, P. Arvan, M. Tchórzewski, M.D. Snider, M. Puchowicz, C.M. Croniger, S.R. Kimball, T. Pan, A.E. Koromilas, R.J. Kaufman, M. Hatzoglou, A self-defeating anabolic program leads to β-cell apoptosis in endoplasmic reticulum stress-induced diabetes via regulation of amino acid flux *, J. Biol. Chem. 288 (24) (2013) 17202–17213.
[60] M.L. Golson, J.C. Dunn, M.F. Maulis, P.K. Dadi, A.B. Osipovich, M.A. Magnuson, D. A. Jacobson, M. Gannon, Activation of FoxM1 revitalizes the replicative potential of aged β-cells in male mice and enhances insulin secretion, Diabetes 64 (11) (2015) 3829–3838.
[61] D.B. Davis, J.A. Lavine, J.I. Suhonen, K.A. Krautkramer, M.E. Rabaglia, J. M. Sperger, L.A. Fernandez, B.S. Yandell, M.P. Keller, I.M. Wang, E.E. Schadt, A. D. Attie, FoxM1 is up-regulated by obesity and stimulates beta-cell proliferation, Molecular endocrinology (Baltimore, Md 24 (9) (2010) 1822–1834.
[62] H. Zhang, A.M. Ackermann, G.A. Gusarova, D. Lowe, X. Feng, U.G. Kopsombut, R. H. Costa, M. Gannon, The FoxM1 transcription factor is required to maintain pancreatic β-cell mass, Mol. Endocrinol. 20 (8) (2006) 1853–1866.
[63] M.T. Malecki, U.S. Jhala, A. Antonellis, L. Fields, A. Doria, T. Orban, M. Saad, J. H. Warram, M. Montminy, A.S. Krolewski, Mutations in NEUROD1 are associated with the development of type 2 diabetes mellitus, Nat. Genet. 23 (3) (1999) 323–328.
[64] F.J. Naya, H.P. Huang, Y. Qiu, H. Mutoh, F.J. DeMayo, A.B. Leiter, M.J. Tsai, Diabetes, defective pancreatic morphogenesis, and abnormal enteroendocrine differentiation in BETA2/neuroD-deficient mice, Genes Dev. 11 (18) (1997) 2323–2334.
[65] G. Matsumoto, K. Wada, M. Okuno, M. Kurosawa, N. Nukina, Serine 403 phosphorylation of p62/SQSTM1 regulates selective autophagic clearance of ubiquitinated proteins, Mol. Cell 44 (2) (2011) 279–289.
[66] H. Peng, J. Yang, G. Li, Q. You, W. Han, T. Li, D. Gao, X. Xie, B.-H. Lee, J. Du, J. Hou, T. Zhang, H. Rao, Y. Huang, Q. Li, R. Zeng, L. Hui, H. Wang, Q. Xia, X. Zhang, Y. He, M. Komatsu, I. Dikic, D. Finley, R. Hu, Ubiquitylation of p62/sequestosome1 activates its autophagy receptor function and controls selective autophagy upon ubiquitin stress, Cell Res. 27 (5) (2017) 657–674.
[67] B. Carroll, E.G. Otten, D. Manni, R. Stefanatos, F.M. Menzies, G.R. Smith, D. Jurk, N. Kenneth, S. Wilkinson, J.F. Passos, J. Attems, E.A. Veal, E. Teyssou, D. Seilhean, S. Millecamps, E.-L. Eskelinen, A.K. Bronowska, D.C. Rubinsztein, A. Sanz, V. I. Korolchuk, Oxidation of SQSTM1/p62 mediates the link between redox state and protein homeostasis, Nat. Commun. 9 (1) (2018) 256.
[68] C. Wilson, C. González-Billault, Regulation of cytoskeletal dynamics by redox signaling and oxidative stress: implications for neuronal development and trafficking, Front. Cell. Neurosci. 9 (2015), 381-381.

[69] Y. Samstag, I. John, G.H. Wabnitz, Cofilin: a redox sensitive mediator of actin dynamics during T-cell activation and migration, Immunol. Rev. 256 (1) (2013) 30–47.
[70] E. Balta, J. Kramer, Y. Samstag, Redox regulation of the actin cytoskeleton in cell migration and adhesion: on the way to a spatiotemporal view, Frontiers in Cell and Developmental Biology 8 (1826) (2021).
[71] M. Pignataro, G. Di Rocco, L. Lancellotti, F. Bernini, K. Subramanian, E. Castellini, C.A. Bortolotti, D. Malferrari, D. Moro, G. Valdrè, M. Borsari, F. Del Monte, Phosphorylated cofilin-2 is more prone to oxidative modifications on Cys39 and favors amyloid fibril formation, Redox biology 37 (2020), 101691-101691.
[72] J. Lin, T. Zhou, K. Ye, J. Wang, Crystal structure of human mitoNEET reveals distinct groups of iron–sulfur proteins, Proc. Natl. Acad. Sci. Unit. States Am. 104 (37) (2007) 14640.
[73] M.E. Roberts, J.P. Crail, M.M. Laffoon, W.G. Fernandez, M.A. Menze, M.E. Konkle, Identification of disulfide bond formation between MitoNEET and glutamate dehydrogenase 1, Biochemistry 52 (50) (2013) 8969–8971.
[74] B. Brackeva, V. De Punt, G. Kramer, O. Costa, K. Verhaeghen, G. Stangé, J. Sadones, C. Xavier, J.M.F.G. Aerts, F.K. Gorus, G.A. Martens, Potential of UCHL1 as biomarker for destruction of pancreatic beta cells, Journal of Proteomics 117 (2015) 156–167.
[75] S. Costes, C.-j. Huang, T. Gurlo, M. Daval, A.V. Matveyenko, R.A. Rizza, A.E. Butler, P.C. Butler, β-cell dysfunctional ERAD/ubiquitin/proteasome system in type 2 diabetes mediated by islet amyloid polypeptide-induced UCH-L1 deficiency, Diabetes 60 (1) (2011) 227–238.
[76] S.H. Graham, H. Liu, Life and death in the trash heap: the ubiquitin proteasome pathway and UCHL1 in brain aging, neurodegenerative disease and cerebral Ischemia, Ageing Res. Rev. 34 (2017) 30–38.
[77] S. Hussain, T. Bedekovics, A. Ali, O. Zaid, D.G. May, K.J. Roux, P.J. Galardy, A cysteine near the C-terminus of UCH-L1 is dispensable for catalytic activity but is required to promote AKT phosphorylation, eIF4F assembly, and malignant B-cell survival, Cell Death Discovery 5 (1) (2019) 152.
[78] R. Kumar, D.K. Jangir, G. Verma, S. Shekhar, P. Hanpude, S. Kumar, R. Kumari, N. Singh, N. Sarovar Bhavesh, N. Ranjan Jana, T. Kanti Maiti, S-nitrosylation of UCHL1 induces its structural instability and promotes α-synuclein aggregation, Sci. Rep. 7 (2017), 44558-44558.
[79] J. Duan, M.J. Gaffrey, W.J. Qian, Quantitative proteomic characterization of redox-dependent post-translational modifications on protein cysteines, Mol. Biosyst. 13 (5) (2017) 816–829.
[80] S. Akter, L. Fu, Y. Jung, M.L. Conte, J.R. Lawson, W.T. Lowther, R. Sun, K. Liu, J. Yang, K.S. Carroll, Chemical proteomics reveals new targets of cysteine sulfinic acid reductase, Nat. Chem. Biol. 14 (11) (2018) 995–1004.
[81] H. Xiao, M.P. Jedrychowski, D.K. Schweppe, E.L. Huttlin, Q. Yu, D.E. Heppner, J. Li, J. Long, E.L. Mills, J. Szpyt, Z. He, G. Du, R. Garrity, A. Reddy, L.P. Vaites, J. A. Paulo, T. Zhang, N.S. Gray, S.P. Gygi, E.T. Chouchani, A quantitative tissue-specific landscape of protein redox regulation during aging, Cell 180 (5) (2020) 968–983 e24.
[82] J. Duan, T. Zhang, M.J. Gaffrey, K.K. Weitz, R.J. Moore, X. Li, M. Xian, B.D. Thrall, W.J. Qian, Stochiometric quantification of the thiol redox proteome of macrophages reveals subcellular compartmentalization and susceptibility to oxidative perturbations, Redox biology 36 (2020) 101649.
[83] T. Zhang, M.J. Gaffrey, X. Li, W.J. Qian, Characterization of cellular oxidative stress response by stoichiometric redox proteomics, Am. J. Physiol. Cell Physiol. 320 (2) (2021) C182–C194.
[84] K. Wolhuter, H.J. Whitwell, C.H. Switzer, J.R. Burgoyne, J.F. Timms, P. Eaton, Evidence against stable protein S-nitrosylation as a widespread mechanism of post-translational regulation, Mol. Cell. 69 (3) (2018) 438–450, e5.
[85] I. Gusarov, E. Nudler, Protein S-nitrosylation: enzymatically controlled, but intrinsically unstable, post-translational modification, Mol. Cell. 69 (3) (2018) 351–353.
[86] C.-C. Chou, B.-Y. Chiang, J.C.-Y. Lin, K.-T. Pan, C.-H. Lin, K.-H. Khoo, Characteristic tandem mass spectral features under various collision chemistries for site-specific identification of protein S-glutathionylation, J. Am. Soc. Mass Spectrom. 26 (1) (2015) 120–132.
[87] J.D. Majmudar, B.R. Martin, Strategies for profiling native S-nitrosylation, Biopolymers 101 (2) (2014) 173–179.
[88] X.-H. Gao, L. Li, M. Parisien, J. Wu, I. Bederman, Z. Gao, D. Krokowski, S. M. Chirieleison, D. Abbott, B. Wang, P. Arvan, M. Cameron, M. Chance, B. Willard, M. Hatzoglou, Discovery of a Redox Thiol Switch: Implications for Cellular Energy Metabolism, Molecular & Cellular Proteomics, vol. 19, 2020, pp. 852–870, 5.
[89] X.-H. Gao, D. Krokowski, B.-J. Guan, I. Bederman, M. Majumder, M. Parisien, L. Diatchenko, O. Kabil, B. Willard, R. Banerjee, B. Wang, G. Bebek, C.R. Evans, P. L. Fox, S.L. Gerson, C.L. Hoppel, M. Liu, P. Arvan, M. Hatzoglou, Quantitative H2S-mediated protein sulfhydration reveals metabolic reprogramming during the integrated stress response, eLife 4 (2015) e10067-e10067.
[90] S. Lu, S.-B. Fan, B. Yang, Y.-X. Li, J.-M. Meng, L. Wu, P. Li, K. Zhang, M.-J. Zhang, Y. Fu, J. Luo, R.-X. Sun, S.-M. He, M.-Q. Dong, Mapping native disulfide bonds at a proteome scale, Nat. Methods 12 (4) (2015) 329–331.
[91] J.C. Lakbub, J.T. Shipman, H. Desaire, Recent mass spectrometry-based techniques and considerations for disulfide bond characterization in proteins, Anal. Bioanal. Chem. 410 (10) (2018) 2467–2484.
[92] S. Jiang, L. Carroll, L.M. Rasmussen, M.J. Davies, Oxidation of protein disulfide bonds by singlet oxygen gives rise to glutathionylated proteins, Redox biology 38 (2021) 101822.
[93] N.J. Day, M.J. Gaffrey, W.J. Qian, Stoichiometric thiol redox proteomics for quantifying cellular responses to perturbations, Antioxidants 10 (3) (2021).
[94] W. Arif, S. Xu, D. Isailovic, W.J. Geldenhuys, R.T. Carroll, M.O. Funk, Complexes of the outer mitochondrial membrane protein mitoNEET with resveratrol-3-sulfate, Biochemistry 50 (25) (2011) 5806–5811.
[95] A.R. Huehn, J.P. Bibeau, A.C. Schramm, W. Cao, E.M. De La Cruz, C.V. Sindelar, Structures of cofilin-induced structural changes reveal local and asymmetric perturbations of actin filaments, Proc. Natl. Acad. Sci. U. S. A. 117 (3) (2020) 1478–1484.
[96] D.H. Kwon, O.H. Park, L. Kim, Y.O. Jung, Y. Park, H. Jeong, J. Hyun, Y.K. Kim, H. K. Song, Insights into degradation mechanism of N-end rule substrates by p62/SQSTM1 autophagy adapter, Nat. Commun. 9 (1) (2018) 3291.